High aspect ratio nanoimprinted grooves of poly(lactic-co-glycolic acid) control the length and direction of retraction fibers during fibroblast cell division

Citation	Su, Y. H., Chiang, P. C., Cheng, L. J., Lee, C. H., Swami, N. S., & Chou, C. F. (2015). High aspect ratio nanoimprinted grooves of poly (lactic-co-glycolic acid) control the length and direction of retraction fibers during fibroblast cell division. Biointerphases, 10(4), 041008. doi:10.1116/1.4936589
DOI	10.1116/1.4936589
Publisher	Springer
Version	Version of Record
Terms of Use	http://cdss.library.oregonstate.edu/sa-termsofuse

High aspect ratio nanoimprinted grooves of poly(lactic-co-glycolic acid) control the length and direction of retraction fibers during fibroblast cell division

Yi-Hsuan Su[a)]
Institute of Physics, Academia Sinica, Taipei 11529, Taiwan and Department of Electrical and Computer Engineering, University of Virginia, Charlottesville, Virginia 22904

Po-Chieh Chiang[a)]
Institute of Physics, Academia Sinica, Taipei 11529, Taiwan

Li-Jing Cheng
Institute of Physics, Academia Sinica, Taipei 11529, Taiwan and School of Electrical Engineering and Computer Science, Oregon State University, Corvallis, Oregon 97331

Chau-Hwang Lee
Research Center for Applied Sciences, Academia Sinica, Taipei 11529, Taiwan and Institute of Biophotonics, National Yang-Ming University, Taipei 11221, Taiwan

Nathan S. Swami[b)]
Department of Electrical and Computer Engineering, University of Virginia, Charlottesville, Virginia 22904

Chia-Fu Chou[b)]
Institute of Physics, Academia Sinica, Taipei 11529, Taiwan; Research Center for Applied Sciences, Academia Sinica, Taipei 11529, Taiwan; and Genomics Research Center, Academia Sinica, Taipei 11529, Taiwan

(Received 23 August 2015; accepted 5 November 2015; published 9 December 2015)

Retraction fibers (RFs) determine orientation of the cell division axis and guide the spreading of daughter cells. Long and unidirectional RFs, which are especially apparent during mitosis of cells in three-dimensional (3D) environments, enable improved control over cell fate, following division. However, 3D gel environments lack the cues necessary for predetermining the orientation of RFs to direct tissue architecture. While patterning of focal adhesion regions by microcontact printing can determine orientation of the RFs through enhancing focal adhesion numbers along particular directions, the RFs remain short due to the two-dimensional culture environment. Herein, the authors demonstrate that nanoimprinted grooves of polylactic acid glycolic acid (PLGA) with a high aspect ratio (A.R. of 2.0) can provide the cues necessary to control the direction of RFs, as well as enable the maintenance of long and unidirectional RFs as observed within 3D cultures, while the same is not possible with PLGA grooves of lower A.R. (1.0 or lower). Based on enhanced levels of contact guidance of premitotic fibroblast protrusions at high A.R. grooves and deeper levels of focal adhesion due to filopodia extensions into these grooves, it is suggested that submicron (800 nm width) PLGA grooves with A.R. of 2 are capable of supporting mechanical forces from cell protrusions to a greater depth, thereby enabling the maintenance of the protrusions as long and unidirectional RFs during cell division. Given the scalability and versatility of nanoimprint techniques, the authors envision a platform for designing nanostructures to direct tissue regeneration and developmental biology. © *2015 American Vacuum Society*. [http://dx.doi.org/10.1116/1.4936589]

I. INTRODUCTION

The control of cell division is crucial for determining cell fate and tissue architecture within embryogenesis and morphogenesis.[1] For instance, orientation of the epithelial cell division axis is important in maintaining epithelial integrity, since misoriented divisions can give rise to daughter cells that lie above or below the epithelial layer.[2] New blood vessel formation requires the coordination of endothelial cell divisions, which can effectively extend blood vessels.[3] Similarly, controlling the cell division axis of fibroblasts, which align within the wound bed along the secreted collagen fibers and the extracellular matrix (ECM), can determine tissue regeneration and architecture during wound healing.[4] Orientation of the cell division axis is determined by the spatial distribution of contact adhesion regions, mechanical forces from the retraction fibers (RFs) and the cortical cues developed during interphase.[5] RFs are the membrane tubes filled with actin filaments that connect the cells undergoing round-up during mitosis, to the underlying adhesive substrate through integrins.[6] The anisotropy of cell geometry during interphase is one of the key factors that determine the orientation of the cell division axis. When a cell is

[a)]Y.-H. Su and P.-C. Chiang contributed equally for this work.
[b)]Authors to whom correspondence should be addressed; electronic addresses: nswami@virginia.edu; cfchou@phys.sinica.edu.tw

constrained within a geometry, the mitotic spindles align along the longest axis of the elongated cell morphology;[7] however, its final orientation is determined by the cues associated with retraction fibers during cell rounding. In a 2D culture, the rounded mitotic cells show no or only short RFs of differing orientation that are linked through integrins to the substrate,[8,9] which limits their anisotropy. On the other hand, when the cells are embedded in 3D fibrin gels,[9] the dividing cells round-up only around the cell body, while exhibiting long and polarized RFs that connect the cell body to the matrix, for supporting anisotropic mechanical forces toward improved guidance of daughter cells and determination of tissue architecture. However, although the daughter cells respread along the direction of the RFs in the 3D fibrin gel, the original orientation of the RFs cannot be predetermined. In order to control the orientation of the mitotic spindles, previous studies have patterned ECM proteins by using microcontact printing to act as focal adhesion regions for the control of mitotic orientation. However, unlike the long and unidirectional RFs in 3D culture, the confinement of mitotic cells within 2D patterns causes multiple short RFs connected to the patterned ECM regions;[7,8] which limits their spatial extent for guidance. One method to enhance the contact guidance on cells due to a particular pattern is to increase the aspect ratio (A.R. or depth/width) of the pattern;[10–13] however, its role in influencing the cell division axis and guidance of daughter cells over long extent has not been elucidated within prior work. Hence, in this current study, we seek to utilize high aspect ratio topographic features patterned on biodegradable polymers that are suitable for tissue regeneration, such as polylactic acid glycolic acid (PLGA), to provide the necessary cues for predetermining the orientation of cell division, as well as toward maintaining long and unidirectional RFs for effectively guiding daughter cells.

Various techniques have been utilized to fabricate anisotropic patterned structures for studying cell division within a constrained geometry. Microcontact printing of ECM proteins confines cells within a pattern.[5,7,8] However, other than constraining cell culture to two dimensions, the spatial anisotropy of this method is limited by surface diffusion of the printed proteins and it requires alignment procedures for the mold to the desired area. Polarized laser irradiation to generate periodic surface structures has been investigated.[14] However, precise control of the aspect ratio of the topography is challenging, and the background scattering of the light can cause topographic uncertainties. Another method is based on generating a spatial gradient of a self-assembled monolayer of ECM ligand peptides by utilizing permeation and diffusion in a microfluidic device. However, the working area for controlling the cell division axis is limited to the region with the highest range of peptide densities.[15] The application of electron-beam lithography (EBL) for creating patterns to study cell–substrate interactions[16,17] is limited by the incompatibility of EBL resists to cell culture environments and the inability of EBL to fabricate nanoscale features over millimeter-scale surface areas, which is time-consuming. Electrospinning is a template-free method to produce nanoscale fiber structures and tubular structures over a large area,[18–22] but it is difficult to pattern and orient electrospun nanofibers. Hence, we choose nanoimprint lithography (NIL) to fabricate PLGA nanogrooves of varying A.R., since NIL can precisely pattern nanostructures over a large surface area on biodegradable polymers, with highly controlled A.R. and reproducibility.[23–25]

In this study, we show that during mitosis, fibroblasts on PLGA grooves with an A.R. of 1.0 or lower, exhibit complete round-up with little or no RFs, resembling prior cell division observations on 2D patterned substrates. On the other hand, on nanoimprinted grooves with an A.R. of 2.0, the cells maintain long and unidirectional RFs during cell round-up that enhance anisotropy during cell division, similar to observations on cells cultured in a 3D fibrin gel. This enhanced anisotropy provides the cues to determine the cell division axis and guide daughter cells over large spatial extents. Due to their enhanced contact guidance of premitotic protrusions and deeper filopodia extensions, we suggest that nanoimprinted PLGA grooves of submicron scale width (800 nm) and A.R. 2, provide the physical cues for supporting mechanical forces to a greater depth, from long and unidirectional retraction fibers during cell round-up. Based on the scalability of nanoimprint techniques on a variety of biocompatible polymeric substrates, we envision their application toward the design of high-aspect ratio nanostructures for directing tissue architecture, with cell microenvironments that resemble those within 3D culture.

II. EXPERIMENTAL METHODS

A. Fabrication of the PLGA nanogrooves

PLGA (Aldrich, 85:15, MW = 50 000–75 000) was dissolved in a mixture of tetrahydrofuran and dimethylformamide in a 1:1 volume ratio to make a 15% w/v solution. Glass coverslips were cleaned by a standard RCA cleaning procedure (using a mixture of NH_4OH, H_2O_2, and H_2O in a 1:1:5 volume ratio at 80 °C) for 10 min to remove organic contamination. A PLGA film with a thickness of 1.3 μm was spun onto a glass coverslip for fabricating the grooves by NIL techniques. The imprinting process was conducted at 100 °C (the glass transition temperature of PLGA is 45–50 °C)[26] under a pressure of 50 bars for 300 s by using a silicon mold in an Obducat Eitre3 machine. Prior to cell experiments, we examined all the PLGA nanogrooves by using an atomic force microscope (AFM, Veeco Bioscope II). Table I lists the feature dimensions of the nanogrooves used in this study.

B. Cell culture

NIH3T3 fibroblasts were cultured at 37 °C and 5% CO_2 in Dulbecco's modified Eagles medium containing 100 units/ml penicillin, and 100 μl/ml and 10% calf serum (Gibco). The patterned PLGA substrate was sterilized by UV light for 30 min before seeding the cells. The cells were seeded at a

TABLE I. Aspect ratios of the topographical dimensions of nanoscale and submicron scale PLGA grooves. The pitch of the grooves equals their width to enable appropriate aspect ratio comparisons.

		Width (w)		
Aspect ratio (d/w)		200 nm	400 nm	800 nm
Depth (d)	50 nm	0.25	0.125	
	100 nm	0.5	0.25	0.125
	200 nm	1	0.5	0.25
	400 nm	2	1	0.5
	800 nm		2	1
	1600 nm			2

density $\sim 10^3\,\mathrm{cm}^{-2}$ onto the PLGA substrate and cultured for 48 h, prior to observation.

C. Immunofluorescent staining

We followed the manufacturer's instructions for the staining processes. In brief, the culture medium was removed after incubation and the cells were washed with phosphate buffered saline (PBS). After fixation in 4% paraformaldehyde for 1 h, the cells were permeabilized with 0.1% Triton X-100 in PBS for 3 min and blocked by 1% bovine serum albumin in PBS for 20 min. The cells were then incubated with Alexa Fluor 488 conjugated phalloidin (Invitrogen) and Hoechst 3332 at room temperature in dark for 20 min to stain the actin filaments and the nuclei, respectively. The stained cells were observed by using an inverted optical microscope (Olympus X71), equipped with Olympus color charge coupled device (CCD) for the images in Fig. S1,[27] and Andor electron multiplying CCD camera (iXon DV897) for the images in Fig. 2. To access cell adhesion on the PLGA surface, we stained the fibroblasts with the primary monoclonal antibody to mouse vinculin (Millipore) and rhodamine-conjugated secondary antibody. The stained cells were washed with PBS and then fixed by using the ProLong® Gold Antifade Reagent (Invitrogen) to enhance resistance to photobleaching. The vinculin images were acquired with a confocal microscope (Leica TCS SP5).

D. Time-lapse microscopy of live cells

For temporal analyses of the movement of individual cells, the fibroblasts were cultured on either a patterned or nonpatterned substrate, which was fixed onto the bottom of a culture dish by doubled-sided tape. Cells were seeded at 1×10^3 cells/cm^2/100 μl onto the substrate to allow for attachment on the substrates in a 37 °C, 5% CO_2 incubator for 4 h. A computer program automatically recorded phase contrast images of the NIH3T3 fibroblasts for 72 h with a 10-min interval. Movies were assembled in the NIH IMAGEJ software package and were imported into METAMORPH NX software to plot the cell trajectories and to calculate the cell migration speeds.

E. Statistical analysis

For all data reported herein, three independent experiments were performed in triplicate condition per study. Cell migration trajectories in Fig. S4 (Ref. 27) were analyzed for statistical significance using two-way analysis of variance (ANOVA) with the corresponding function in Microsoft Excel. A p value <0.05 was considered significant.

III. RESULTS

A. Cell division on PLGA grooves with A.R. ≤ 2

PLGA grooves were fabricated by nanoimprint lithography (Fig. 1), with grooves of so-called nanoscale (100, 200, and 400 nm) and submicron scale widths (800 nm), which were chosen to enable penetration of cell filopodia. We begin with an examination of the cell division process, including the premitotic phase, mitosis, and respreading of

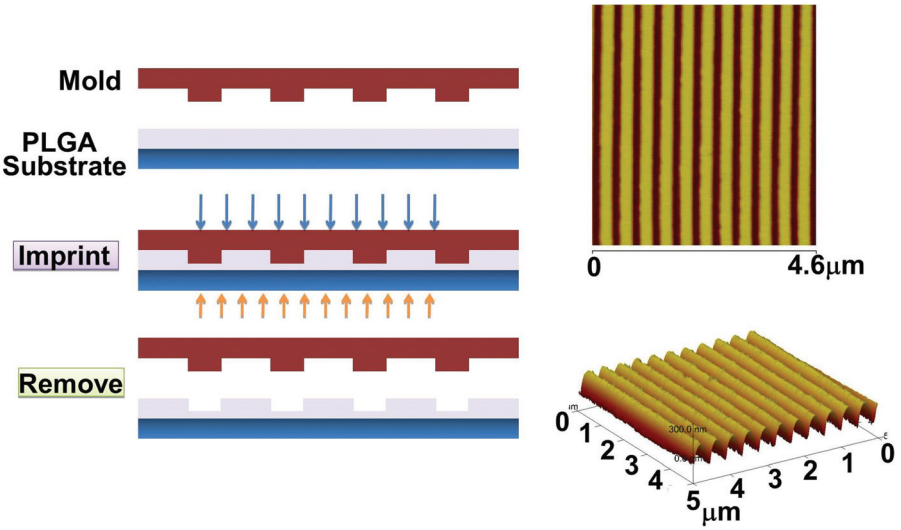

FIG. 1. Nanoimprint lithography process for PLGA grooves and example AFM image of the imprinted pattern (200 nm depth and 200 nm width) on the substrate.

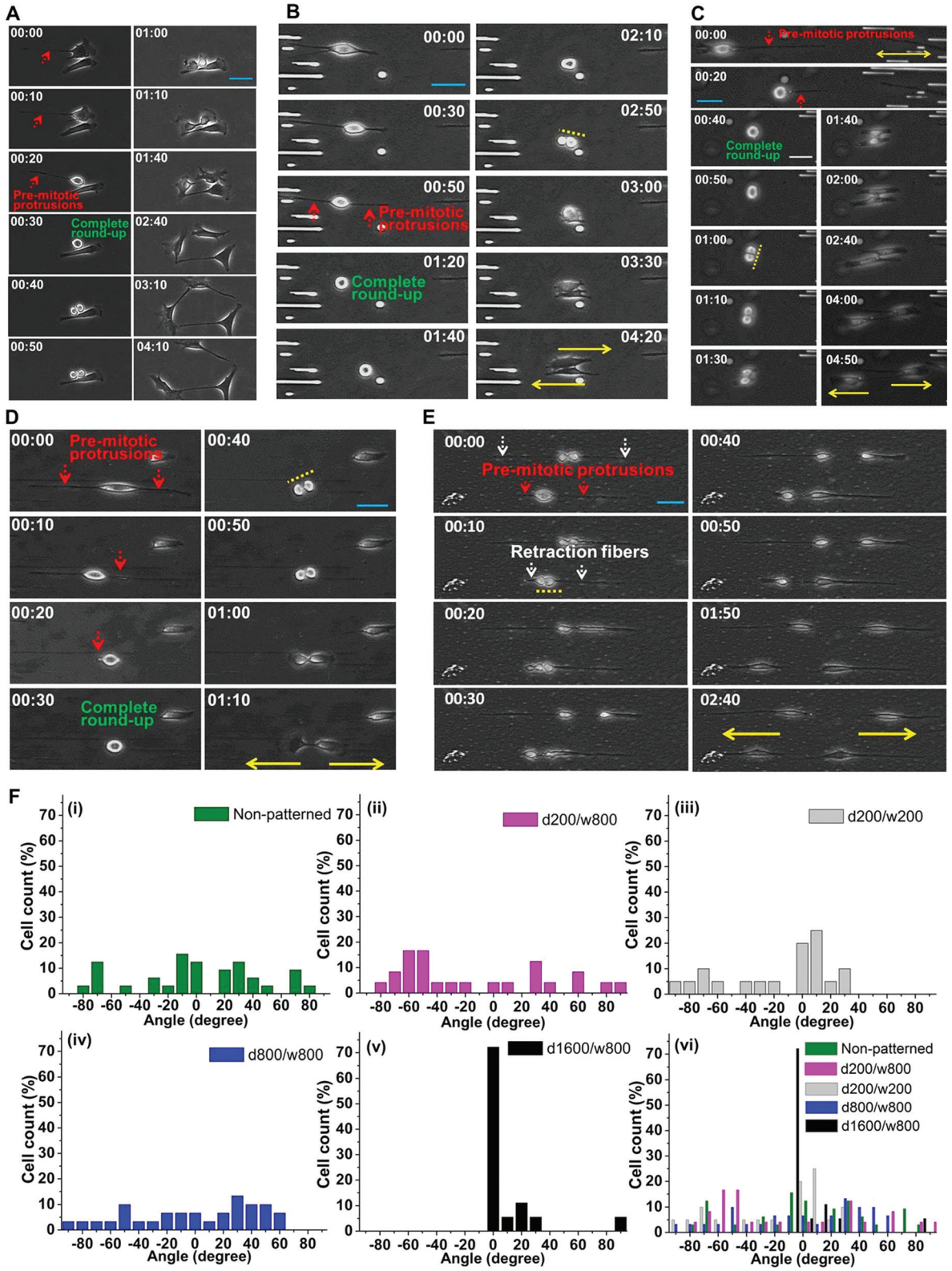

FIG. 2. Time-lapse images (timing "hour:minute") of morphology during cell division on nonpatterned (a) and patterned grooves with A.R. (depth/width) of 0.25: (b) 200/800 (depth/width); A.R. of 1.0: (c) 200/200 (depth/width) nm and (d) 800/800 nm; and with an A.R. of 2.0: (e) 1600/800 nm. Movies of cell division at A.R. of 2.0, 1.0 and lower are available in supplementary material (Ref. 27). The red arrows indicate premitotic protrusions, the yellow dotted line indicates orientation of cell division, the white dotted arrows indicate RF, and the yellow solid arrows indicate cell migration aligned along the direction of the grooves. Scale bar (blue), 50 μm. (f) Angular distributions of the cell division axis vs the orientation of premitotic protrusions on nonpatterned (i), and patterned grooves with an A.R. of 0.25: (ii) 200/800 nm (depth/width), A.R. of 1.0: (iii) 200/200 nm and (iv) 800/800 nm; and angular distributions of the cell division axis vs the orientation of RF with an A.R. of 2.0: (v) 1600/800 nm (premitotic protrusions become RFs). (vi) A comparison of angular distributions of the cell division axis vs the orientation of premitotic protrusions and the orientation of RF (for 1600/800 nm grooves).

the daughter cells on PLGA substrates, with varying AR of the topography. Specifically, using time-lapse videos shot at 10 min intervals (videos are available in supplementary material),[27] we compare the cell dynamics on: (1) nonpatterned PLGA substrates [Fig. 2(a)]; (2) submicron scale PLGA grooves with an A.R. of 0.25 [200 nm depth/800 nm width in Fig. 2(b)]; (3) nanoscale PLGA grooves with A.R. of 1.0 [200 nm depth/200 nm width in Fig. 2(c)]; (4) submicron scale PLGA grooves with an A.R. of 1 [800 nm depth/800 nm width in Fig. 2(d)]; and (5) submicron scale PLGA grooves with an A.R. of 2 [1600 nm depth/800 nm width in Fig. 2(e)].

On the nonpatterned substrate [Fig. 2(a)], the cell in the premitosis phase develops a distinctive polarity during interphase, with lamellipodia at the leading edge and the premitotic protrusions at the trailing edge of the cell (red dotted arrows). During mitosis, the cell starts to round-up, and the lamellipodia and tail retract (note the image at 00:30), with complete round-up in cell morphology and no distinct RFs. Following the mitosis, within 10 min, the daughter cells start to spread along random directions on the substrate, with cell lamellipodia actively exploring their surrounding area. These obvious morphological alterations of fibroblasts during mitosis, from their original spindle-shaped morphology during premitosis to complete cell round-up prior to division, indicate that fibroblasts are good candidates for gauging the onset of division toward quantifying the influence of various patterned topographies. On submicron grooves of A.R. 0.25 [Fig. 2(b)], the elongated cell morphology during the premitotic phase (at 00:50), as apparent from the aligned premitotic protrusions (red dotted arrows) along the direction of the grooves (yellow arrows), is converted to a rounded morphology with no apparent RFs during mitosis (at 02:50). On nanoscale grooves of A.R. 1 [Fig. 2(c)], the elongated cell morphology during the premitotic phase (at 00:00), as apparent from the aligned premitotic protrusions (red dotted arrows) along the direction of the grooves (yellow arrows), is converted to a rounded morphology with no apparent RFs during mitosis (at 00:40). Hence, the elongated cell morphology on the nanoscale grooves during interphase does not provide the necessary cues to generate RFs for connecting the rounded cell to the substrate and for guiding orientation of the cell division axis (at 01:00, yellow dotted line) [see Fig. 2(c), and supplementary material, Movie S1[27]]. In fact, 55 out of 56 cells undergo complete round-up during mitosis on nanoscale grooves of A.R. 1. Similar results are observed on the submicron scale grooves with an A.R. of 1 [Fig. 2(d)], wherein the elongated morphology during interphase does not provide the cues to generate RFs, as apparent from the lack of connection between the mitotic cells and the substrate [00:30 vs 00:40 in Fig. 2(d)], seen within each of the 20 analyzed cells. In contrast, on submicron scale grooves with an A.R. of 2, the elongated premitotic protrusions during interphase are maintained as long and unidirectional RFs during mitosis [white dotted lines in Fig. 2(e)], so that the anisotropy is maintained at the edges and round-up occurs only within the cell body. After cell division, the daughter cells immediately migrate along this long and unidirectional RF, which is aligned to the grooves (supplementary material, Movie S2[27]). In fact, 22 out of 23 analyzed cells on submicron scale PLGA grooves with an A.R. of 2, display long and unidirectional RFs during mitosis, oriented to the grooves [standard deviation (SD) = 2.67°], with an average length of 166 ± 60 μm and average width of 2.88 ± 0.66 μm. It is noteworthy that in contrast to their random directions on the nonpatterned substrate [Fig. 2(a)], the respective premitotic protrusions on patterned substrates are aligned along the direction of the grooves [Figs. 2(b)–2(e)] and localized at the tip of the leading edge of the cell, causing the cells to move along the direction of the grooves with a slow retracted trailing edge, leading to a highly elongated morphology, with a very distinct polarity. As per Fig. 2(f), the orientation angle of the RF direction versus cell division axis on 1600/800 nm (depth/width) submicron grooves exhibits a narrow distribution between ±10°, with a notable peak of more than 70% counts at 0°, indicating highly effective cell division guidance via RF. In contrast, the orientation angles between premitotic protrusion versus cell division axis on nonpatterned, 200/200 and 800/800 nm nanogrooves exhibit no preferred alignment. It is noteworthy that although there is about 20%–30% counts between ±10°, all the cells undergo complete round-up during mitosis, as shown in supplementary material, Movie S1.[27]

B. Contact guidance of the premitotic protrusions on PLGA grooves

To understand the cues that lead to the maintenance of long and unidirectional RFs during cell division on submicron scale PLGA grooves of high-aspect ratio, we study the premitotic protrusions on grooves as a function of the topographic features. Specifically, we characterize their contact guidance on grooves of varying width and aspect ratio, as quantified by their alignment and elongation. To assess the degree of alignment on the grooves, we analyze the SDs of the orientation angles of premitotic protrusions (with an average at 0°) for 200 nm (blue column), 400 nm (red column), and 800 nm (green column) width grooves at the mentioned A.R. in Fig. 3(a), with the respective value of the nonpatterned substrate serving as the control (SD = 51.0°). Representative images of their morphology, as well as the angular distribution of their orientation on 200 nm width grooves of varying A.R. versus those on nonpatterned substrates, can be found in the supplementary Fig. S1.

While the premitotic protrusions are well aligned on grooves of 100 nm width and depth (SD = 16.5°) versus on the nonpatterned substrate (SD = 51.0°), the alignment is successively higher on 200 and 400 nm width grooves at an A.R. of 1.0, as evident from the smaller SDs of the orientation angles. However, no further improvement in alignment is observed on nanoscale PLGA grooves at an A.R. of 2.0. On the other hand, on so-called submicron scale grooves of 800 nm width, the alignment is successively improved for structures up to an A.R. of 2.0, where the lowest SDs of the

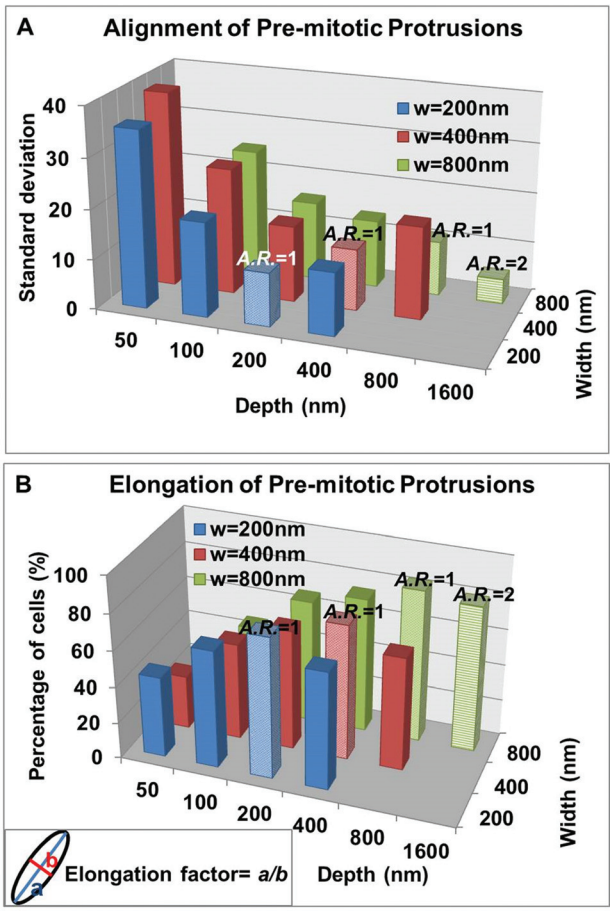

FIG. 3. Alignment and elongation of premitotic protrusions on grooves of various widths and depths. (A): The values of SDs represent the degree of alignment of premitotic protrusions on the respective grooves. Each data point is from measurements on 750 cells. (B): The percentage of premitotic protrusions with an elongation factor larger than that of the cells cultured on nonpatterned (N-p) substrate (mean ± SD). The elongation factor is defined by the ratio (a/b) of the longest axis (a) of a cell to the maximum perpendicular width (b). Each data point is from the measurements on 300 cells. A separated graph for the comparisons of each width can be found in the supplementary Fig. S2.[27]

orientation angles are observed. The elongation factor is assessed by measuring the ratio of the longest axis of the entire cell body to its maximum perpendicular width, as defined in Fig. 3(b). Since the average elongation factor of 300 cells on the nonpatterned substrate is 11 ± 6.1, we count the percentages of cells on the patterned grooves that exhibit an elongation factor larger than 11, as shown in Fig. 3(b). It is apparent that the elongation trend tracks that of the degree of alignment of the protrusions, confirming maximum elongation for 200 and 400 nm width grooves at an A.R. of 1.0, with no further elongation at the higher A.R. of 2.0 [blue and red column in Fig. 3(b), respectively], whereas the elongation on 800 nm width submicron scale grooves continues to increase up until the highest A.R. of 2.0 that is used within this study [green column in Fig. 3(b)]. In fact, the highest elongation is observed on submicron scale (800 nm width) grooves with an A.R. of 2.0, where ~85% of the cells with premitotic protrusions show elongation factors greater than 11.

C. Deeper focal adhesions on PLGA grooves with A.R. of 2

Cell filopodia are known to play a crucial role in sensing the topographic features.[28] Hence, we seek to characterize the depth variations of focal contacts from the premitotic cell protrusions on grooves of high versus low A.R., using z-stacks of their confocal images to examine the distribution of vinculin-positive focal adhesions. Specifically, we examine the actin organization and distribution of vinculin, which stabilizes focal adhesion.[29] Vinculin is localized and activated during the extension of premitotic protrusions,[30] and it has been shown to play an important role in the structural integrity of filopodia. The data are shown for periodic displacements of 200 nm along the depth, downward from the top surface of the grooves.

A representative image of the cell protrusions on the grooves with an A.R. of 1.0 is shown in Fig. 4(a). The vinculin-positive focal adhesion distribution at the tip, and on either side of the cells, is clearly apparent in the first focal plane, wherein the top surface of the groove pattern is apparent. The vinculin signals continue to be apparent at the 200 and 400 nm depth focal planes, but are only vaguely apparent at the 600 and 800 nm depth focal planes. However, the vinculin-positive focal adhesion signals from the cell protrusions on the grooves with an A.R. of 2.0 substrates appear clearly down to the 800 nm depth focal plane [Fig. 4(b)]. The vinculin-positive focal adhesion numbers from cell protrusions at grooves with A.R. 1.0 vs 2.0 are quite similar [Fig. 4(c)]. Here, the presence of vinculin-positive focal adhesion is confirmed by fluorescence intensity levels greater than a threshold level (using NIH IMAGEJ software), as set by the mean fluorescence intensity of each image plus two standard deviations.[30] Representative fluorescent images can be found in supplementary Fig. S3.[27] To quantify the distribution of vinculins on the grooves with an A.R. of 1.0 vs 2.0, we calculate the percentage of cells with vinculin-positive focal adhesions at each focal plane. The presence of vinculin-positive focal adhesions is confirmed by fluorescence intensity levels greater than a threshold level, as set by the mean fluorescence intensity of each image plus two standard deviations. On the grooves with an A.R. of 1.0, only 10% of the 30 measured cells contain vinculin-positive focal adhesions beyond the 400 nm depth focal plane, whereas on the grooves with an A.R. of 2.0, more than 50% of cells are found to contain vinculin-positive focal adhesions down to the 800 nm depth focal plane [Fig. 4(d)]. Hence, even though vinculin-positive focal adhesion numbers from premitotic cell protrusions are similar for the grooves with an A.R. of 2.0 vs A.R. of 1.0 [Fig. 4(c)], we infer the deeper extension of filopodia into grooves with an A.R. of 2.0, based on the depth distribution of vinculin [Fig. 4(d)].

IV. DISCUSSION

RFs are known to exert strong mechanical forces on mitotic cells and the underlying substrate, thereby providing

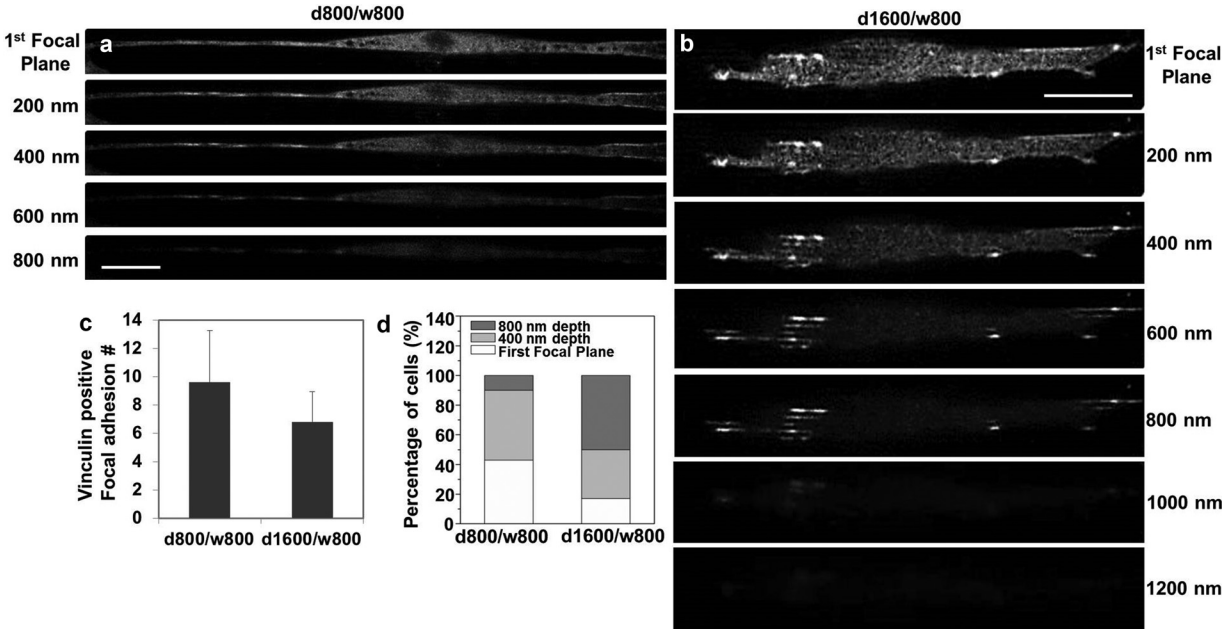

FIG. 4. Z-stacks of confocal images of intracellular vinculin to quantify filopodia penetration into grooves with an A.R. of 1.0 vs 2.0. The images are taken from the highest focal plane (top surface of the groove patterns) downwards every 200 nm until the vinculin signal is undetectable. (a) The prominent vinculin spots on the protrusion of the cells are seen from the highest focal plane until 400 nm depth on grooves with an A.R. of 1.0 substrates (800/800). (b) The vinculin spots on the protrusion of the cells are seen onwards from the 200 nm down to 800 nm depth focal planes, on the grooves with an A.R. of 2.0 substrates (1600/800). (c) Vinculin-positive focal adhesion numbers for the cells on each substrate type. (d) Quantification of the percentage of cells with vinculin signals exceeding the threshold, imaged at various depths on each substrate type (calculated from 30 cells). Scale bar, 20 μm.

physical cues from the substrate toward inducing spindle rotation and alignment. As a result, RFs can determine the orientation of the cell division axis and the direction for guiding daughter cells,[1,7,8] thereby controlling tissue architecture. Long RFs capable of supporting large and highly anisotropic mechanical forces are apparent during mitosis for cells cultured within 3D matrices, whereas cells in 2D matrices do not show significant RFs, and hence lack mechanisms for guiding daughter cells.[9] However, the direction of these RFs and the orientation of the cell division axis cannot be predetermined for cells cultured within 3D gel matrices, thereby causing daughter cells to spread along RFs, which can occur along random directions. Based on our observations of fibroblast cell division [Fig. 2(e)], nanoimprinted PLGA grooves with an A.R. of 2.0 (1600 nm depth/800 nm lateral width), not only exhibit the cues for maintaining long and unidirectional RFs similar to cells cultured within 3D matrices, but also enable the predetermination of the direction of RFs and orientation of the cell division axis based on the direction of the underlying grooves. In this manner, nanoimprinted PLGA grooves with a high A.R. can maintain the premitotic cell protrusions as long RFs during the cell round-up phase of mitosis and thereby guide the respreading of daughter cells over large distances ($\sim$166 μm) to control tissue architecture. On the other hand, PLGA grooves with an A.R. of 1 (at 200, 400 or 800 nm lateral width) are unable to provide the cues for maintaining the premitotic cell protrusions as RFs during the cell round-up phase of mitosis. We correlate this observation to the enhanced levels of contact guidance of the premitotic fibroblast protrusions at high A.R. PLGA grooves [Figs. 3(a) and 3(b)] and deeper levels of focal adhesion into the structure of high A.R. PLGA grooves (Fig. 4), as apparent from deeper protrusion of filopodia. Filopodia, which are expressed by mitotic cells at elevated levels,[31] can steer the mother cell toward 3D topographic features during mitosis.[28] Hence, we suggest that through enabling the deeper extension of filopodia, high A.R. nanoimprinted PLGA grooves of submicron width are able to support mechanical forces to a greater depth, similar to prior work,[32,33] thereby providing the cues to avoid the detachment of premitotic cell protrusions during the cell round-up phase of division and enabling their maintenance as long and unidirectional RFs. Finally, it is noteworthy that this methodology of using high A.R. nanoimprinted PLGA grooves to guide RFs during mitosis differs considerably from previous work,[5,8] using microcontact printing of fibronectin for patterning focal adhesions to direct RFs and guide daughter cells. The microcontact printing approach increases the focal adhesion numbers along a particular patterned region, thereby enabling a number of short RFs for orienting cell division and guiding daughter cells. On the other hand, our approach based on high A.R. nanoimprinted PLGA grooves enables focal adhesions over a greater depth [Fig. 4(d)], rather than by increasing focal adhesion numbers, which remain similar for A.R. 2 vs A.R. 1 grooves [Fig. 4(c)]. In this manner, through supporting mechanical forces over greater depths, the high A.R. groove structure provides cues for maintaining long and unidirectional RFs during mitosis, thereby controlling the orientation of cell division and enhancing the spatial extent for guiding the spreading of daughter cells.

ACKNOWLEDGMENTS

The authors thank technical support from the Academia Sinica Nano Core Facilities. This work was supported by the Academia Sinica Research Program on Nanoscience and Nanotechnology, Academia Sinica Integrated Thematic Project (AS-103-TP-A01), the Minister of Science and Technology, Taiwan (102-2112-M-001-005-MY3 and 103-2923-M-001-007-MY3), Asian Office for Aerospace Research and Development (No. FA2386-12-1-4002), and USA NSF Award No. 1332329.

[1]X. Morin and Y. Bellaiche, Dev. Cell **21**, 102 (2011).
[2]D. T. Bergstralh, T. Haack, and D. St Johnston, Philos. Trans. R. Soc., B **368**, 20130291 (2013).
[3]G. Zeng, S. M. Taylor, J. R. McColm, N. C. Kappas, J. B. Kearney, L. H. Williams, M. E. Hartnett, and V. L. Bautch, Blood **109**, 1345 (2007).
[4]H. N. Kim, Y. Hong, M. S. Kim, S. M. Kim, and K. Y. Suh, Biomaterials **33**, 8782 (2012).
[5]M. Thery and M. Bornens, Curr. Opin. Cell Biol. **18**, 648 (2006).
[6]C. H. Streuli, J. Cell Sci. **122**, 171 (2009).
[7]M. Thery, V. Racine, A. Pepin, M. Piel, Y. Chen, J. B. Sibarita, and M. Bornens, Nat. Cell Biol. **7**, 947 (2005).
[8]J. Fink *et al*., Nat. Cell Biol. **13**, 771 (2011).
[9]A. Lesman, J. Notbohm, D. A. Tirrell, and G. Ravichandran, J. Cell Biol. **205**, 155 (2014).
[10]W. Hu, E. K. Yim, R. M. Reano, K. W. Leong, and S. W. Pang, J. Vac. Sci. Technol., B **23**, 2984 (2005).
[11]P. Uttayarat, G. K. Toworfe, F. Dietrich, P. I. Lelkes, and R. J. Composto, J. Biomed. Mater. Res. **75A**, 668 (2005).
[12]S. A. Fraser, Y. H. Ting, K. S. Mallon, A. E. Wendt, C. J. Murphy, and P. F. Nealey, J. Biomed. Mater. Res. **86A**, 725 (2008).
[13]A. S. Crouch, D. Miller, K. J. Luebke, and W. Hu, Biomaterials **30**, 1560 (2009).
[14]X. Wang, C. A. Ohlin, Q. Lu, and J. Hu, Biomaterials **29**, 2049 (2008).
[15]B. M. Lamb, W. Luo, S. Nagdas, and M. N. Yousaf, ACS Appl. Mater. Interfaces **6**, 11523 (2014).
[16]D. H. Kim, K. Han, K. Gupta, K. W. Kwon, K. Y. Suh, and A. Levchenko, Biomaterials **30**, 5433 (2009).
[17]T. Dvir, B. P. Timko, D. S. Kohane, and R. Langer, Nat. Nanotechnol. **6**, 13 (2011).
[18]N. S. Swami, Z. Cui, and L. S. Nair, J. Heat Transfer **133**, 034002 (2010).
[19]V. Chaurey, P. C. Chiang, C. Polanco, Y. H. Su, C. F. Chou, and N. S. Swami, Langmuir **26**, 19022 (2010).
[20]V. Chaurey, F. Block, Y. H. Su, P. C. Chiang, E. Botchwey, C. F. Chou, and N. S. Swami, Acta Biomater. **8**, 3982 (2012).
[21]A. Nandakumar *et al*., Small **9**, 3405 (2013).
[22]R. A. Neal, S. S. Tholpady, P. L. Foley, N. Swami, R. C. Ogle, and E. A. Botchwey, J. Biomed. Mater. Res. **100A**, 406 (2012).
[23]L. J. Guo, X. Cheng, and C. F. Chou, Nano Lett. **4**, 69 (2004).
[24]H. N. Kim, D. H. Kang, M. S. Kim, A. Jiao, D. H. Kim, and K. Y. Suh, Ann. Biomed. Eng. **40**, 1339 (2012).
[25]M. Elsayed and O. M. Merkel, Nanomedicine **9**, 349 (2014).
[26]L. Singh, V. Kumar, and B. D. Ratner, Biomaterials **25**, 2611 (2004).
[27]See supplementary material at http://dx.doi.org/10.1116/1.4936589 for movies on cell trajectories during division on the grooves, as well as for alignment and elongation of pre-mitotic protrusions on PLGA grooves.
[28]J. Albuschies and V. Vogel, Sci. Rep. **3**, 1658 (2013).
[29]J. T. Parsons, A. R. Horwitz, and M. A. Schwartz, Nat. Rev. Mol. Cell Biol. **11**, 633 (2010).
[30]J. D. Humphries, P. Wang, C. Streuli, B. Geiger, M. J. Humphries, and C. Ballestrem, J. Cell Biol. **179**, 1043 (2007).
[31]M. A. Partridge and E. E. Marcantonio, Mol. Biol. Cell **17**, 4237 (2006).
[32]A. I. Teixeira, G. A. Abrams, P. J. Bertics, C. J. Murphy, and P. F. Nealey, J. Cell Sci. **116**, 1881 (2003).
[33]J. R. Sun, Y. F. Ding, N. J. Lin, J. Zhou, H. Ro, C. L. Soles, M. T. Cicerone, and S. Lin-Gibson, Biomacromolecules **11**, 3067 (2010).